

PREPARATION AND CHARACTERIZATION OF PETI-330/MULTIWALLED CARBON NANOTUBE

Sayata Ghose,¹ Kent A. Watson,² Dennis C. Working,³ Jim M. Criss,⁴ Emilie J. Siochi,³ John W. Connell³

¹National Research Council Research Associate located at
NASA LaRC, Hampton, VA 23681

²National Institute of Aerospace
100 Exploration Way, Hampton, VA 23666

³NASA Langley Research Center
Hampton, VA 23681-2199

⁴M & P Technologies, Inc.
Marietta, GA 30068

ABSTRACT

As part of an ongoing effort to incorporate multifunctionality into advanced composites, blends of PETI-330 and multi-walled carbon nanotubes (MWCNTs) were prepared, characterized and fabricated into moldings. The PETI-330/MWCNT mixtures were prepared at concentrations ranging from 3 to 25 weight percent by dry mixing the components in a ball mill. The resulting powders were characterized for degree of mixing, thermal and rheological properties. Based on the characterization results, PETI-330/MWCNT samples were scaled up to ~300 g and used to fabricate moldings 10.2 cm x 15.2 cm x 0.32 cm thick. The moldings were made by injecting the mixtures at 260-280 °C into an Invar[®] tool followed by curing for 1 h at 371 °C. The tool was designed to impart shear during the injection process in an attempt to achieve some alignment of the MWCNTs in the flow direction. Good quality moldings were obtained that were subsequently characterized for thermal, mechanical and electrical properties. The degree of dispersion and alignment of the MWCNTs were investigated using high-resolution scanning electron microscopy. The preparation and preliminary characterization of PETI-330/MWCNT composites will be discussed.

Keywords: phenylethynyl terminated imides, high temperature polymers, nanocomposites, moldings

This paper is work of the U. S. Government and is not subject to copyright protection in the U.S.

1. INTRODUCTION

Thermally stable, high-performance resins are required for use in composite structures on aerospace vehicles such as supersonic aircraft and reusable launch vehicles. Due to an excellent combination of physical and mechanical properties, aromatic polyimides have emerged as leading candidates for these applications [1, 2]. However, polyimides are difficult to fabricate into composites and in an attempt to improve their processability, controlled molecular weight imide oligomers containing phenylethynyl groups have been developed. These phenylethynyl groups are thermally unreactive up to 300 °C, but react rapidly at temperatures of 350-371 °C without volatile evolution to yield a cross-linked resin [3 - 15]. The combination of a large processing window and the formation of a product exhibiting good toughness, good microcrack resistance and excellent thermo-oxidative stability makes phenylethynyl terminated imide (PETI) technology very attractive for use in high performance composite and adhesive applications. PETI-330 is a low molecular weight imide oligomer that has a low and stable melt viscosity at 280 °C and a glass transition temperature of 330 °C after curing at 371 °C. It has been used for making good quality composites by resin transfer molding (RTM), vacuum-assisted RTM (VARTM) and resin infusion (RI) [9,10].

Material needs on some advanced aerospace vehicles such as Gossamer spacecraft require multifunctional capabilities. For example, incorporating carbon nanotubes (CNTs) into aromatic polyimide films provides sufficient electrical conductivity to dissipate electrostatic charge (ESC) buildup without degrading mechanical properties and flexibility or significantly compromising the optical properties [16]. When CNTs are thoroughly dispersed in the polymeric material, an interconnecting structure of CNTs is formed which provides a pathway for electrical charge to flow. Various methods have been employed for achieving good dispersion of CNTs in the polymer including the preparation of the polymer in the presence of CNTs under sonication [17] and the use of alkoxysilane terminated amide acid oligomer to disperse the CNTs [18]. In applications where only surface conductivity is required, single-walled carbon nanotubes (SWCNTs) were spray-coated on the surface of polymer substrates [16]. In all these experiments, CNT concentration was minimized in order to retain the desired optical properties of the films.

Unlike thin films needed for Gossamer spacecraft, structural components do not require optical transparency or low color. Thus the incorporation of multi-walled nanotubes (MWCNTs), which are less expensive and have lower aspect ratio compared to SWCNTs, was investigated for structural and electrical applications. The goal of this research was to incorporate a sufficient concentration of MWCNTs to affect electrical conductivity and modulus improvement without severely reducing the melt flow properties (i.e., processability) of the matrix resin. The approach taken involves using a dry mixing technique for incorporating MWCNTs. Maintaining melt flow properties is important because melt processing is generally the preferred method of fabricating composites. However the process has not been extensively used for nanocomposites because CNTs tend to form agglomerates under these conditions and at high loading levels the viscosity becomes too high for processing. Usually, this can be minimized by the appropriate application of shear during mixing. For example, polymethylmethacrylate (PMMA) containing SWCNTs has been produced using a combined method of solvent casting and melt mixing [19]. In this method small pieces of cast films were pressed between heated plates and the resulting film was again broken many times. The entire method was repeated several times and the film obtained by

this method had a more homogeneous distribution of nanotubes and better mechanical properties than the original film. A miniature mixer-molder has also been used to produce small quantities of well-dispersed mixtures of MWCNT in PMMA [20]. The mixtures were then compressed into thin films and measurements of their dynamic mechanical behavior showed an increase in storage modulus.

Another recent method to disperse MWCNTs uses a micro-scale twin-screw extruder for the melt mixing of MWCNTs with polycarbonates [21] and polystyrene [22]. The high shear mixing necessary to disentangle and uniformly disperse MWCNTs in the matrix can be achieved with the extruder. The process of extruding the nanocomposite through a suitable die and subsequent drawing leads to continuous ribbons of nanocomposites that can be further processed into laminates. Alignment of nanotubes by drawing from the polymer melt resulted in significant improvements in elastic modulus and yield strength when compared to randomly oriented nanocomposites [22]. Morphological studies using transmission electron microscopy (TEM) and scanning electron microscopy (SEM) have shown interconnecting structures formed by the nanotubes that efficiently helps in load transfer between the polymer matrix and nanotube reinforcement [21, 22]. SWCNTs have been incorporated (up to 1 % by weight) into Ultem™ 1000, a thermoplastic polyetherimide, and melt processed to yield fibers [23]. Although the melt process was not optimized to fully disperse and align the SWCNTs some improvements in mechanical properties were achieved. Typically melt processing works better for thermoplastics than thermosets due to melt stability in the required processing window. However, oligomers endcapped with phenylethynyl groups possess the appropriate combination of processing characteristics for melt processes like injection molding or extrusion.

Ball-milling is a mechanical process that leads to local generation of high pressure as a result of the collision between the grinding media [24]. This method has been used to obtain nano-barrels from cup-stacked carbon nanotubes [25], transform nanotubes to nanoparticles (ellipsoidal and spherical) [26], generate nanostructures from graphite [27 - 28] and shorten the lengths of nanotubes [29 - 30]. Polyethylene terephthalate (PET) was compounded with various grades (5 wt %) of carbon nanofibers (CNF) by ball-milling [31] followed by extrusion or melt mixing but to date there is no reported work on dry compounding of polymers with MWCNTs using the ball mill.

The successful fabrication of nanocomposites that contain high loadings (>3 % by weight) of CNTs has been elusive. The objective of this research was to combine PETI-330 with high loadings of MWCNTs using a dry mixing technique like ball-milling prior to fabricating nanocomposites by injection molding. Preparation of samples containing various loading levels of MWCNTs followed by their characterization are presented in this paper. Based on the properties, select samples were chosen for injection molding and the molded plaques were subsequently characterized.

2. EXPERIMENTAL

2.1 Preparation of PETI-330/MWCNT by dry mixing

Dry mixing of PETI-330 and MWCNTs was carried out in alumina-fortified porcelain jars using cylindrically shaped zirconia grinding media (9.5 mm x 9.5 mm). The jars were placed on rollers

(120 rotations per min) and rotated for 48 h. Initially, the mixing was done on a small scale using 0.4 L capacity jars. Mixtures containing 3, 5, 7, 10, 12, 15, 20 and 25 wt % MWCNTs were prepared. Based on the melt rheology and other characterization, two samples were chosen for scale up using a 1.9 L jar. After mixing, the powder was separated from the grinding media by a sieve. Typical recovery yields ranged from 70 – 80 % of the total weight due to adhesion of the powder to the jar and grinding media.

2.2 Composite Specimens of PETI-330/MWCNT

An Invar[®] tool designed such that the injection ports are tapered to provide shear during injection, which may lead to some orientation of the MWCNTs, was used in the fabrication of moldings. Approximately 300 g of PETI-330/MWCNT sample was degassed in the injector by heating to 280 °C and holding for 1 h prior to injection. The high temperature injector was built by Radius Engineering according to Lockheed Martin specifications and can operate at a maximum temperature of 288°C, flow rate of 500 cc/min, and pressure of 2.75 MPa. The degassing step is generally required in RTM primarily to remove moisture and air from the material. After the resin was injected at 288 °C at a rate of 200 cc/min, the tool was held in a press at a minimum of 1.38 MPa of hydrostatic pressure in order to assure adequate sealing, heated to 371 °C and held at this temperature for 1 h. The plaques were cooled in the mold.

2.3 Characterization

Differential scanning calorimetry (DSC) was performed on the powder samples obtained from ball-milling using a Shimadzu DSC-50 thermal analyzer at a heating rate of 20 °C/min with the T_g taken as the mid-point of inflection of the differential heat flow (ΔH) versus temperature curve. The samples were cured in a sealed aluminum pan at 371 °C for 1 h, cooled to room temperature and then heated again to 450 °C to determine the T_g . Thermogravimetric analysis (TGA) in air (flow rate – 50 mL/min) was performed on the powder samples using an Auto TGA 2950HR (TA Instruments, DE). The samples were heated at 20 °C/min to 100 °C, held for 30 min to drive off any moisture, and heated to 600 °C at a rate of 2.5 °C/min.

Dynamic rheological measurements were obtained using an Advanced Rheometric Expansion System (ARES) from Rheometrics, Inc. The measurements were carried out under nitrogen in an oscillatory shear mode using parallel plate geometry (30 mm diameter). Discs of the samples were prepared by compression molding approximately 0.75 g of sample at room temperature and subsequently inserted in the test chamber at 100 °C. The top plate was oscillated at a variable strain and a fixed angular frequency of 100 rad/s while the lower plate was attached to a transducer that recorded the resultant torque. The specimens were heated to 280 °C at a rate of 4 °C/min and held at 280 °C for 2 h to assess melt stability. Heating was then continued at the same rate to 371 °C and held for 100 s.

High-resolution SEM images were obtained using a Hitachi S-5200 field emission scanning electron microscope (FE-SEM) equipped with a “through-the-lens” secondary electron detector operating at or below 1 kV. The composite images were obtained in low voltage mode in order to set up a stable local electric field on the sample while minimizing beam-induced damage. Both the powder and the sample obtained from the ARES were scanned. High-resolution TEM was performed with a CM-200 HR-TEM (Philips). Powder samples were dissolved in NMP at 70 °C and PELCO[®] Center-Marked Copper Grids (150 mesh and 3.0 mm O.D.) were dipped in the

solution and characterized by TEM. Neat nanotubes were sonicated in ethanol for 5 min before dipping the grids in the solution. Raman spectroscopy was carried out using a Thermo Nicolet Almega Dispersive Raman spectrometer equipped with a 785 nm laser. The pinhole was 100 μm and the spectral range was $3434 - 72 \text{ cm}^{-1}$. Powder samples were also extruded through a Laboratory Mixing Extruder (LME, Dynisco, MA). The temperature of the mandrel was set at $200 - 210^\circ\text{C}$ and the temperature of the die (1 mm diameter) was set at 230°C . The axial gap size was set at 0.64 mm and the rotor speed was 270 rpm. Elemental analysis of the neat MWCNTs was performed by Desert Analytics (Tucson, AZ) by combustion with the aid of tungsten trioxide (WO_3).

Surface and volume resistivities were measured using a Prostat[®] PRS-801 Resistance System with a PRF-911 Concentric Ring Fixture per ASTM D-257 and reported as an average of three readings. Readings were taken before and after the plaques were polished using a Ecomet-4 Variable Speed Grinder-Polisher. A load of 9.07 kg-force and sanding grids of 60 and 100 were used for polishing. Surface resistance was also measured using a Keithley Sub-Femtoamp Remote Source Meter (Model 6430). Samples were mounted on a Summit 11000/12000 B-Series Probe Station (Cascade Microtech). Distance between the two probes was 0.18 cm and a current of 1 μA was applied.

Thermal conductivity of the plaques was measured using a Netzsch LFA 447 NanoFlash according to ASTM E1461. Samples sizes of 1 cm x 1 cm were sprayed with a thin layer of graphite (for uniform thermal adsorption), which may be easily rinsed away by solvent (e.g. methanol). Pyrex (TC $\sim 1.09 \text{ W/mK}$, Cp $\sim 0.76 \text{ J/gK}$) was used as the reference. Hardness tests were performed on the injection molded plaques using a Wilson Rockwell Hardness Tester (Series 2000). A 1.5875 mm diameter hardened steel ball was used for Test HRT15 with an initial load of 3 kg and a total load of 15 kg. Hardness of the neat resin and composite plaques was also measured using a Shore D durometer according to ASTM D2240 with the plaques being treated as hard plastics. Tensile properties were evaluated using a Sintech 2W and Testworks 4 software with a load cell of 1.334 kN (300 lb-force), crosshead speed of 5.08 mm/min and gauge length of 22 mm. Samples were prepared according to ASTM D1708 specifications and were machined using a Bengal 20 x 40 Water Jet (Flow Corp.).

3. RESULTS AND DISCUSSION

3.1 Melt viscosity of ball-milled PETI-330/ MWCNT samples

The complex viscosity of the neat as well as MWCNT-loaded PETI-330 samples was determined from the rheometer (ARES). Figure 1 shows the melt viscosity curves of neat and MWCNT loaded samples. It is important to note the melt viscosity of samples at a steady temperature of 280°C as the resin is typically injected at this temperature. The neat resin has a low melt viscosity, between 5 and 10 poise (P). At 280°C and a fixed strain rate, the viscosity shows an increasing slope. The phenylethynyl groups do not readily react at this temperature so no significant curing of the resin occurred. This has been tested in the DSC when no reaction was observed on samples held at 280°C for 2 h. As anticipated, when heating was resumed after 2 h, the viscosity decreased with increasing temperature. When the temperature reached $>300^\circ\text{C}$, the phenylethynyl groups started to react and consequently the viscosity increased. For MWCNT-filled samples, melt viscosity was reasonably steady at 280°C and increased with additional

MWCNTs. An exception was in the case of 25 wt % MWCNT filled PETI-330 where the melt viscosity dropped to a value lower than that of the 15 and 20 wt % MWCNT. The reason for this is not clear, but it is possible that at higher loadings the MWCNTs were acting as a lubricant and thus preventing proper friction with the plates of the rheometer resulting in an apparently lower viscosity. It may also be that at higher loadings dispersion is less uniform leading to agglomerates of MWCNTs and an effectively lower viscosity. The melt viscosity for 20 wt % MWCNT is ~28,000 P which is lower than the initial estimated maximum value of 60,000 P for injection molding thus making loadings up to 20 wt % a suitable composition for scale-up.

3.2 HRSEM images of ball-milled PETI-330/ MWCNT samples CNTs tend to form agglomerates which can be minimized by the appropriate application of high shear during mixing. Melt mixing of MWCNTs with various thermoplastics like PMMA, polycarbonate, polypropylene and polyethylene have been successful and SEM images showing the uniform dispersion of nanotubes have been obtained [32 - 33]. However, the only reported work on shear mixing of CNTs and polyimides involves mixing in a mechanical blender for a few minutes [34]. SEM pictures could be obtained only at the highest concentration of 14.3 wt % MWCNTs at an acceleration voltage of 20 kV. Polymers are typically insulating and exposure to the electron beam would cause them to burn. In this work, HRSEM images could be obtained for both powders and samples from the ARES even at a loading level of 5 wt %, indicating a reasonably good dispersion of nanotubes in the polymer matrix to form a conductive network.

Figure 2 shows the HRSEM pictures of neat MWCNTs as well as PETI-330/MWCNT powders obtained after ball-milling. As seen in Figure 2 (b), there is an abundance of MWCNT bundles between polymer particles in the case of 25 wt % loading. However, it was not possible to obtain images of the tube tips at higher magnifications. Typical diameters of individual tubes vary from 30 – 40 nm according to the manufacturer but diameters observed by HRSEM in this study were larger and usually 40 - 200 nm indicating a wide distribution in nanotube size. Figures 2 (c - f) show the images of the samples after testing in the rheometer. Figures 2 (c and d) indicate MWCNT dispersion within the matrix. In Figure 2 (d), the tubes have a bright coating on them which is indicative of a less conductive polymer coating on the nanotube surface. Locations where tubes enter the polymer matrix have a dark circle around them, which arises due to a difference in conductivity of the tubes and the matrix. With the ARES samples it was possible to go to higher magnifications (~60 k) and there was evidence that the tips of some of the tubes were damaged (see Figures 2 e and f). However, it is not certain whether the damage was a result of ball milling or a result of the shearing action of the rheometer followed by fracture of the disc.

3.3 TEM of MWNTs and ball-milled samples TEM images were obtained to examine how ball-milling affected MWCNT structure, if at all. Figure 3 shows images of the nanotubes as received from the University of Kentucky. Ethanol was added to the MWCNTs and the suspension was sonicated for about 5 min, a copper grid was subsequently dipped into the suspension to obtain a thin layer of tubes. There is a hollow channel through the tubes that usually ends before the tip of the tube. Often there were some particles within these channels and Energy Dispersive Spectroscopy (EDS) (Figure 3 (a)) revealed these to be iron (Fe) particles. Iron is typically used as a catalyst during the synthesis of the MWCNTs. A higher magnification (scale: 5 nm) revealed three distinct regions in the image as seen in Figure 3(b). The first is the Fe core of the catalyst particle (dark region), the second is the interface region between the Fe

particle and the carbon, and the third is the carbon encapsulation. There is a distinct change in the distance and direction of the lattice planes in the interface region. The tube walls also showed regions of contrast (see Figure 3 c and d) and on magnification, kinks were found in the walls of the tubes that result in a change in the direction of the lattice planes forming a sieve-like structure. A similar structure with defects in the form of “cross-struts” perpendicular to the axis of the tube has been observed in other neat MWCNTs [35].

Figure 3(e and f) show the images of PETI-330 + 15 wt % MWCNTs after ball-milling. In these images, the resin particles are not observed. The Fe catalyst present in the central channel was also observed in Figure 3(e). On closer examination of the walls, distinct regions that appear like splits (Figure 3 (e)) were seen. Focusing on one such split in Figure 3(f) (scale: 5 nm) it was noticed that the direction of the lattice plane changed immediately following such a split leading to regions of contrast in the image at lower magnifications. Although regions of contrast and change in direction of lattice planes in neat MWCNTs were seen, the splits as seen in Figure 3 (e and f) were not observed. The splits were possibly generated as a result of the ball-milling although catastrophic destruction of the tubes was not seen. Another observation from the TEM images of neat MWCNTs and ball-milled samples was an apparent length reduction in some tubes.

3.4 Raman Spectroscopy The Raman spectra of MWCNTs typically exhibit two optically active phonon modes [36]. The first one is an optically active in-plane stretching E_{2g} mode, the so-called graphite mode, popularly termed as “G” band with a peak around 1580 cm^{-1} . There is another strong band around 1350 cm^{-1} referred to as the “D” band and attributed to disordered graphitic structures. During the manufacturing of CNTs disordered carbonaceous compounds, including amorphous carbon, are produced and these show up in the D-band. As seen in Figure 4, no peak was observed between 1000 to 2000 cm^{-1} for the neat PETI-330. In the case of PETI-330/MWCNT samples with lower concentrations of tubes (3%), both the G and D bands were completely masked by the spectrum of the polymer. Bands were observed at concentrations of 5 wt % or higher and the intensities of both bands increased with increasing nanotube concentration.

3.5 Other characterization Elemental analysis of MWCNTs showed Fe content of ~4 wt % and carbon content of ~96 wt %. The glass transition temperature of neat PETI-330 was $326\text{ }^{\circ}\text{C}$ and only a small change in T_g was observed with the addition of nanotubes. The T_g was $332\text{ }^{\circ}\text{C}$ at 20 wt % MWCNTs were added (Table 1). Thermal degradation data from TGA showed the temperature of 5 wt % loss decreased as the MWCNT content increased. The neat resin lost 5 wt % at $508\text{ }^{\circ}\text{C}$ and the neat MWCNT lost 5 wt % at $512\text{ }^{\circ}\text{C}$, whereas the sample containing 25 wt % MWCNT showed a lower thermal stability losing 5 wt % at $462\text{ }^{\circ}\text{C}$ (Table 1).

3.6 Extrusion of filled nanocomposites The 10, 15 and 20 wt % samples were selected to be scaled up in a 1.9 L jar for further testing that included extrusion. The neat resin and the nanocomposite samples were extruded through a LME. The temperature of the mandrel was between 210 and $215\text{ }^{\circ}\text{C}$ while the die temperature was set at $230\text{ }^{\circ}\text{C}$. It was difficult to obtain continuous fibers of the neat resin even when the die temperature was raised to $300\text{ }^{\circ}\text{C}$. This was due to the low melt viscosity of the resin. In the case of 10 wt % samples, fibers of ~1 m length were extruded at a uniform output rate. Figure 5(a) shows the extruded strands. For 20 wt %

samples, difficulties were encountered during feeding and the rotor temperature rose to 245 °C due to frictional heat buildup. The extrusion of the 15 wt % sample was similar to the 10 wt % sample, but feeding was not always smooth and required occasional manual pressure. Resulting fibers were still very brittle as the resin matrix was not cured. One significant observation was an alignment of nanotubes as a result of extrusion. Figure 5(b) is the HRSEM picture of the 10 wt % extruded fiber surface and most of the tubes were aligned in the direction of fiber extrusion. The orientation of the tubes was more apparent at the end of the fibers as seen in Figure 5(c). It was observed that a majority of the MWCNTs were unidirectionally aligned in the polymer matrix.

3.7 Characterization of Nanocomposite Plaques PETI-330/MWCNT moldings, 10.2 cm x 15.2 cm x 0.32 cm and containing 10 and 15 wt% MWCNT, were prepared by injecting the samples into a specially designed tool (Figure 6) and curing at 371°C for 1 h. When examined under HRSEM, no tubes are observed on the surface of the moldings. However, the sample did not burn indicating that the tubes are probably well dispersed just below the surface. As shown in Figure 7(a), the outline of the tubes can be seen beneath the surface and appear to be aligned in the direction of resin flow as indicated by the arrow. When the fractured edge was examined an abundance of MWCNTs could be observed (see Figure 7 b).

Hardness is the property of a material that enables it to resist plastic deformation, usually by penetration. The hardness testing of plastics is most commonly measured by the Rockwell hardness test or Shore (Durometer) hardness test. Both methods measure the resistance of the plastic towards indentation. Both scales provide an empirical hardness value that does not correlate to other properties or fundamental characteristics. Rockwell hardness is generally chosen for 'harder' plastics such as nylon, polycarbonate, polystyrene, and acetal where the resiliency or creep of the polymer is less likely to affect the results. The data obtained from this test are a useful measure of relative resistance to indentation of various grades of plastics. However, the Rockwell hardness test does not serve well as a predictor of other properties such as strength or resistance to scratches, abrasion, or wear. Both Rockwell and Shore D hardness of the plaques were determined and the values are given in Table 2. The Rockwell hardness number (HR) of a material is given by the equation

$$HR = E - e$$

where e = permanent increase in depth of penetration due to major load, measured in units of 0.001 mm and E = a constant of 100 units for diamond and ball indenters. In this case, the MWCNT-filled samples show a lower hardness value compared to the neat resin. A lower value of HR would mean a greater depth of effective penetration of the indenter or an enhanced plastic deformation of the material.

Surface and volume resistivities (units: Ω/sq) of the plaques were measured as per ASTM D-257 (see Table 3). It was observed that polishing the plaques decreased the resistivity data. The plaque of neat resin was electrically insulating and with increasing concentration of MWCNTs resistivity decreased. Typically for electrostatic charge dissipation to occur, surface resistivity should be between 10^6 and $10^{10} \Omega/\text{sq}$ [37]. With the addition of MWCNTs, the plaques are now in the conductive range. Surface resistivity (units: Ω/cm) was also measured using a two-point probe system. Here, too, the neat samples did not show any conductivity whereas the MWCNT-filled samples were in the conductive range.

Thermal conductivity was measured using Nanoflash and following ASTM E-1461. The instrument allows for direct measurement of thermal diffusivity (α) and a comparative measurement of heat capacity (C_p). The thermal conductivity (λ), is then calculated as $\lambda = \alpha \rho C_p$. Table 4 shows the thermal conductivity data of neat and MWNT-filled samples. With a loading of 10 wt %, conductivity was improved ~3-fold while with 15 wt % loading the improvement is close to 4 times. This suggests that nanotubes are forming an effective network in the polymer matrix which efficiently conducts heat.

Tensile properties were evaluated using a load cell of 1.334 kN (300 lbf), a crosshead speed of 5.08 mm/min and a gauge length of 22 mm. Investigations on the physical appearance of samples were carried out using optical microscopy (Olympus BH-2) at a magnification of 5x. Figure 8 is representative of most samples and shows voids. These voids may be due to volatilization of low molecular weight oligomers within the matrix. PETI-330 was developed as a composite matrix resin and no work has been conducted to optimize the fabrication of neat resin moldings. As a result, during tensile testing the voids act as defect sites that initiate premature mechanical failure, resulting in lower mechanical properties and rendering the data unusable. These measurements were done both in and normal to the flow direction. Because of the defects in these samples, this mechanical data is inconclusive.

4. SUMMARY

The fabrication of nanocomposites containing up to 15 wt % of MWCNTs in a low viscosity, melt stable phenylethynyl terminated imide oligomer (PETI-330) was successfully accomplished. MWCNTs were incorporated into the polyimide matrix by ball-milling without extensive damage to the MWCNTs though evidence of some damage was seen. Select samples were scaled up for processing and continuous strands of nanocomposites were extruded. MWCNTs in the strands showed significant alignment along the direction of extrusion. Plaques were successfully prepared by injecting the material in a specially designed tool and cured at 371 °C for 1 h. PETI-330/MWCNT plaques exhibited increases in both electrical and thermal conductivity and HRSEM showed some alignment of the tubes. MWCNT-filled samples showed a lower hardness value compared to the neat resin. Due to the presence of voids in the samples, mechanical properties were lower than expected. Further work needs to be done to generate void-free samples for better evaluation of mechanical properties.

Acknowledgement

The authors would like to thank Dr. Peter Lillehei of NASA Langley and Dr. Roy Crooks for their help with the HRSEM and HRTEM respectively, Dr. Ravi Shenoy of NASA Langley for hardness measurements and to Mr. Pert Razon of NASA Langley for his help with the ARES. The thermal conductivity measurements by Professor Ya-Ping Sun of Clemson University and the electrical resistivity measurements by Dr. Keun J. Sun of the National Institute of Aerospace are greatly appreciated. They would also like to thank Mr. P. M. Hergenrother and Dr. M. A. Belcher for their valuable discussion.

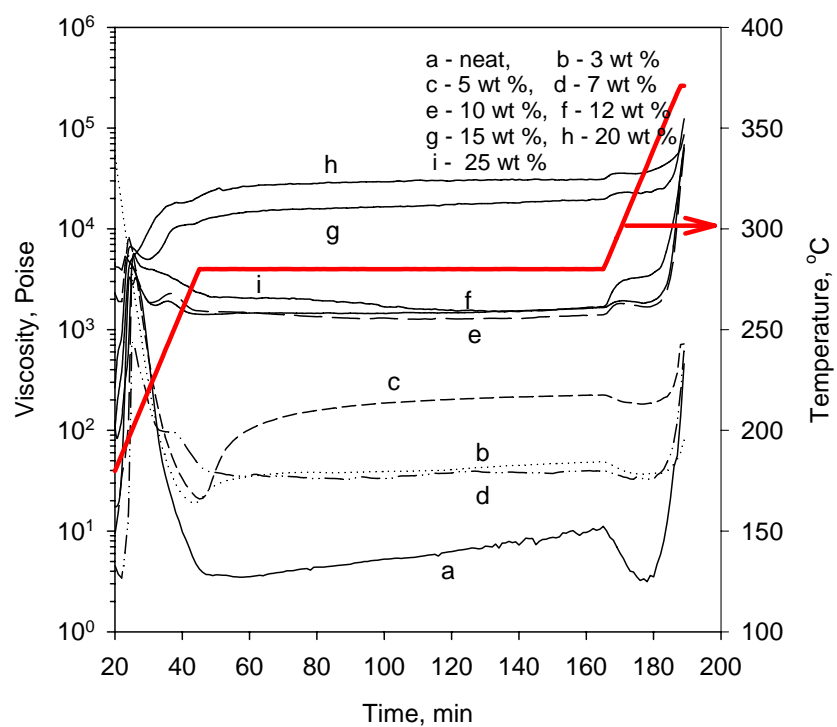
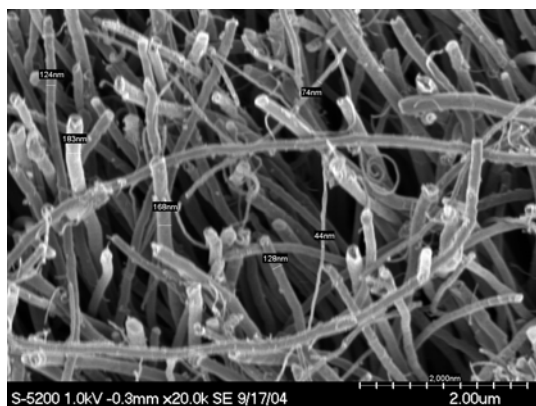
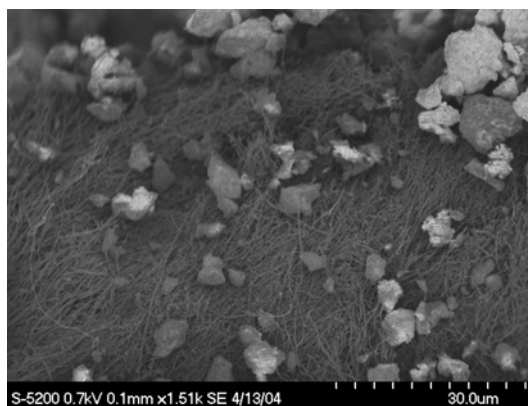


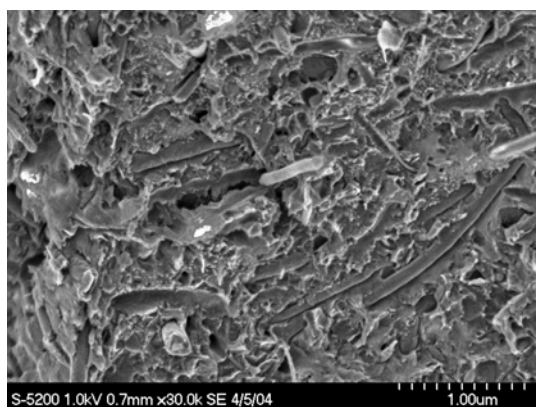
Figure 1: Complex melt viscosity of PETI-330 and various amounts of MWCNT



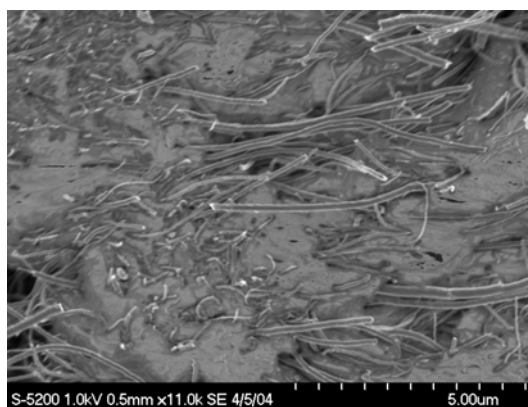
(a) Neat MWCNTs



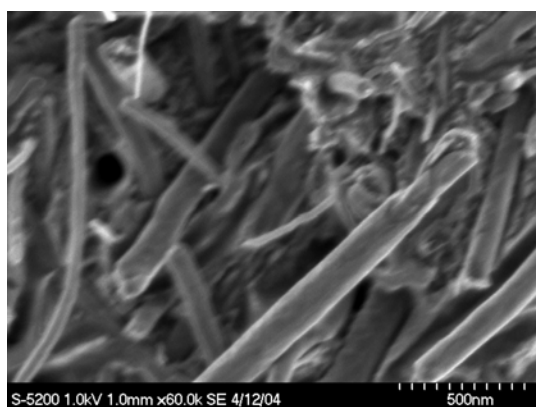
(b) PETI-330 + 25 wt % MWCNT



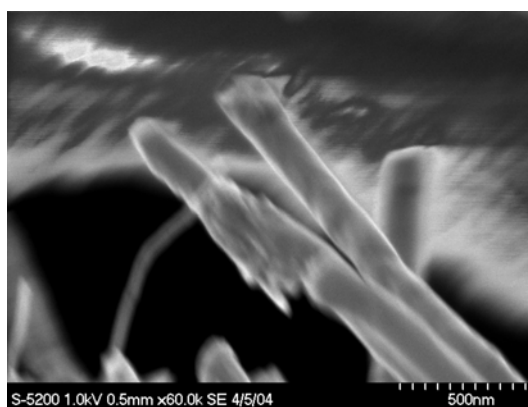
(c) PETI-330 + 10 wt % MWCNT



(d) PETI-330 + 15 wt % MWCNT



(e) PETI-330 + 20 wt % MWCNT



(f) PETI-330 + 15 wt % MWCNT

Figure 2: HRSEM images of neat MWCNTs (a), powder PETI-330/MWCNT samples obtained after ball-milling (b) and PETI-330/MWCNT samples obtained after performing rheology experiments (c-f)

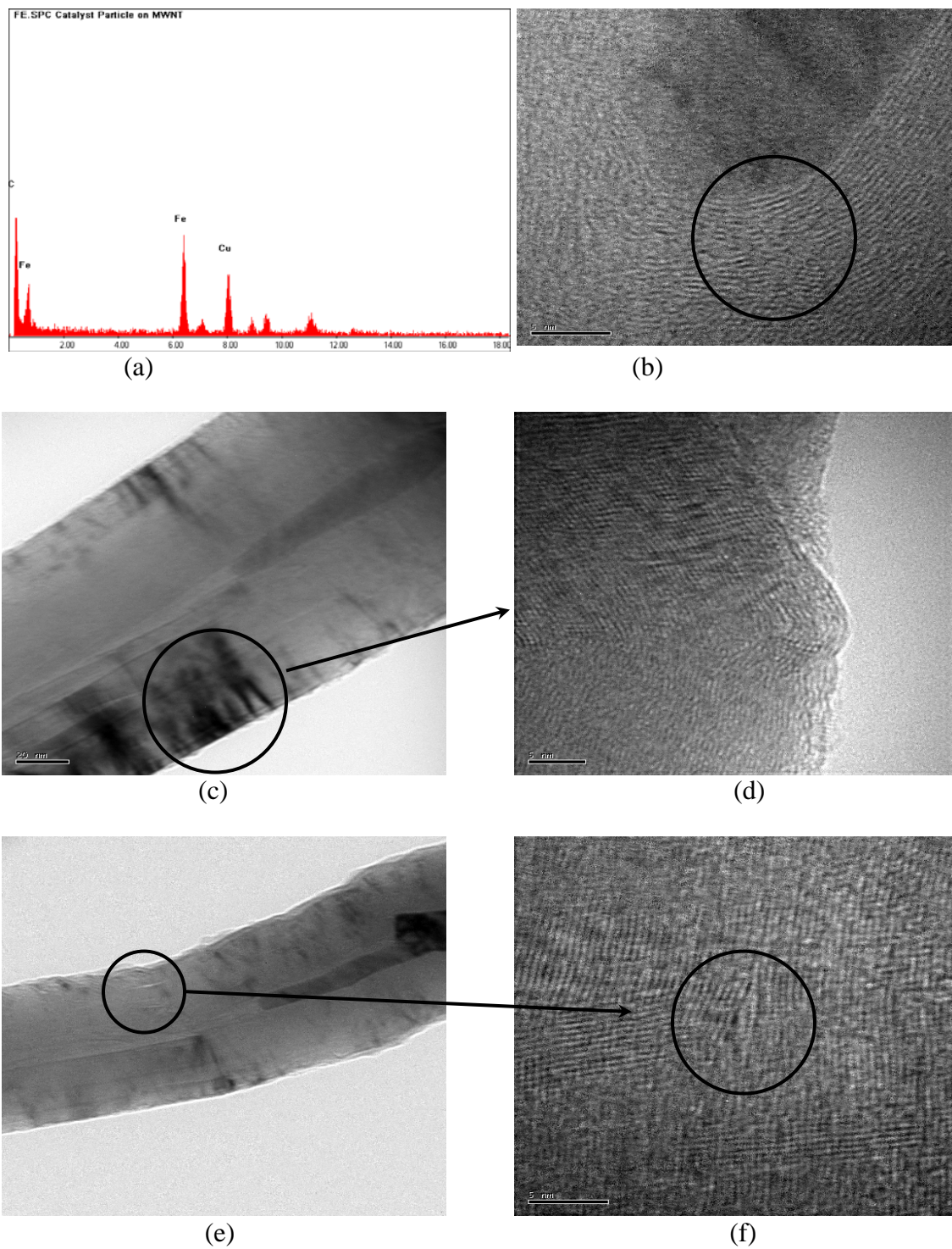


Figure 3: Data (a) and images of neat MWCNTs (b – d) and ball-milled PETI-330 + 15 wt % MWCNTs (e – f) obtained from TEM

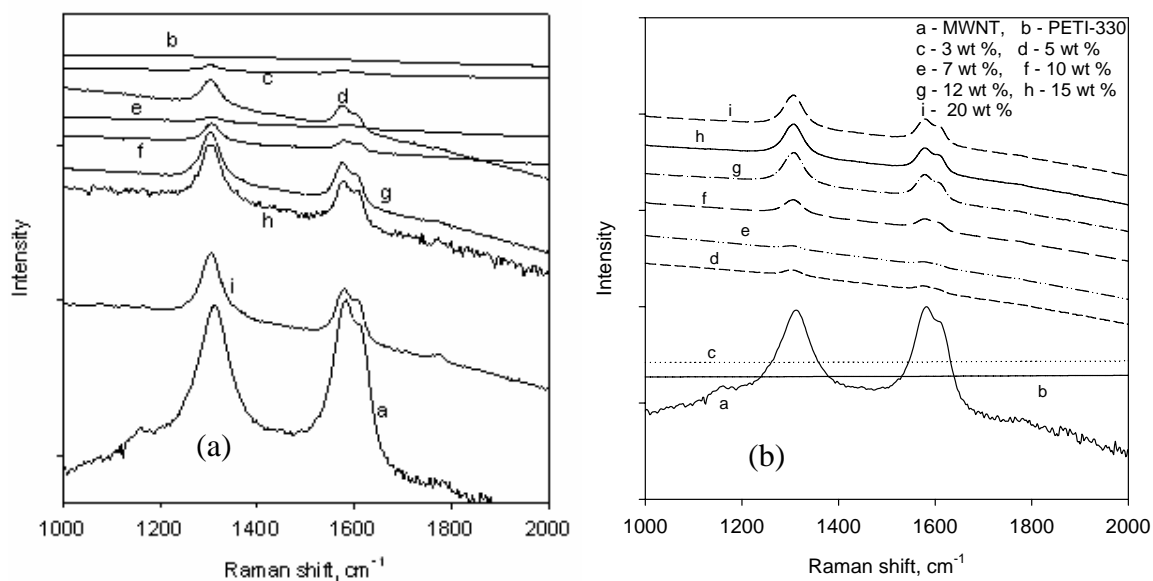


Figure 4: Raman spectra of (a) powder and (b) samples of PETI-330/ MWCNTs after rheology experiments

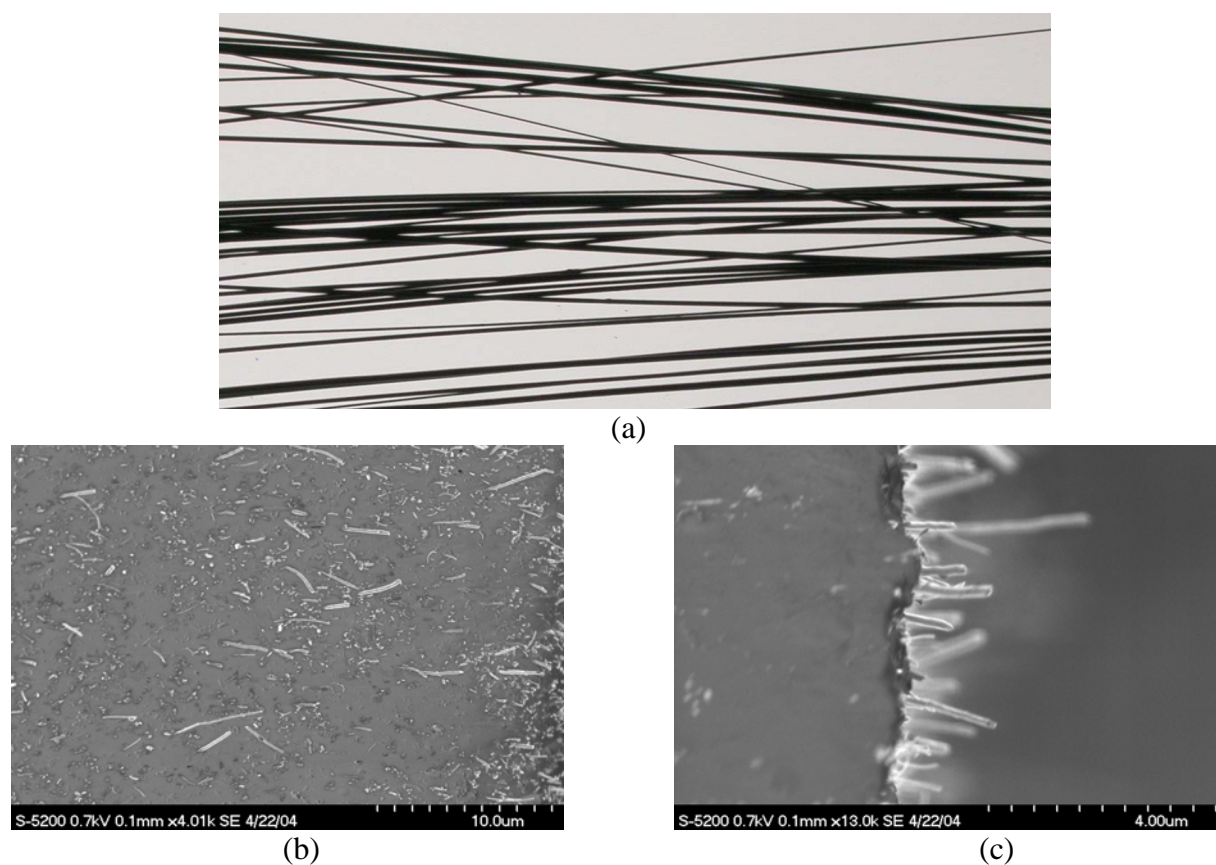


Figure 5: (a) PETI-330/MWCNT (10 wt %) strands after extrusion and (b – c) corresponding HRSEM images

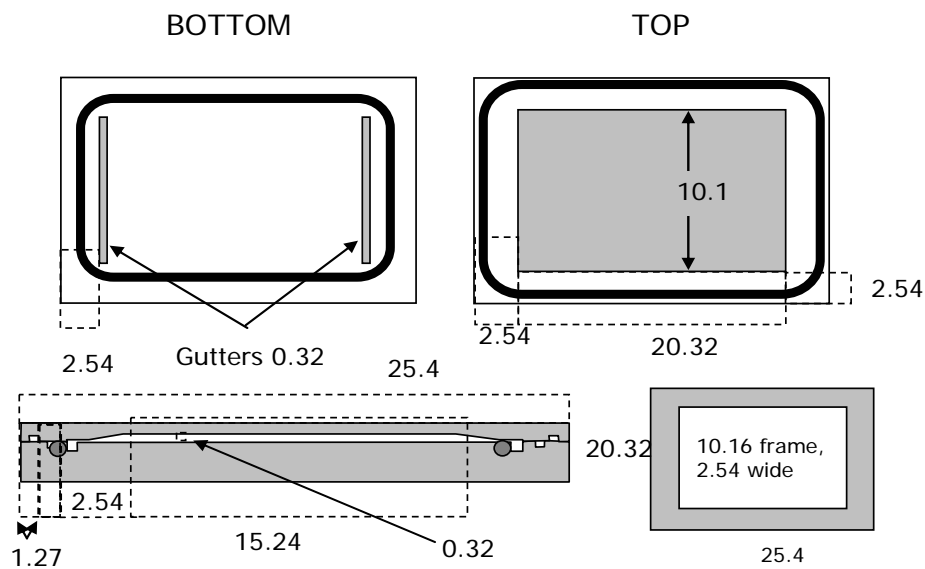


Figure 6: Tool for molding of PETI-330/MWCNT nanocomposites; all dimensions in cm

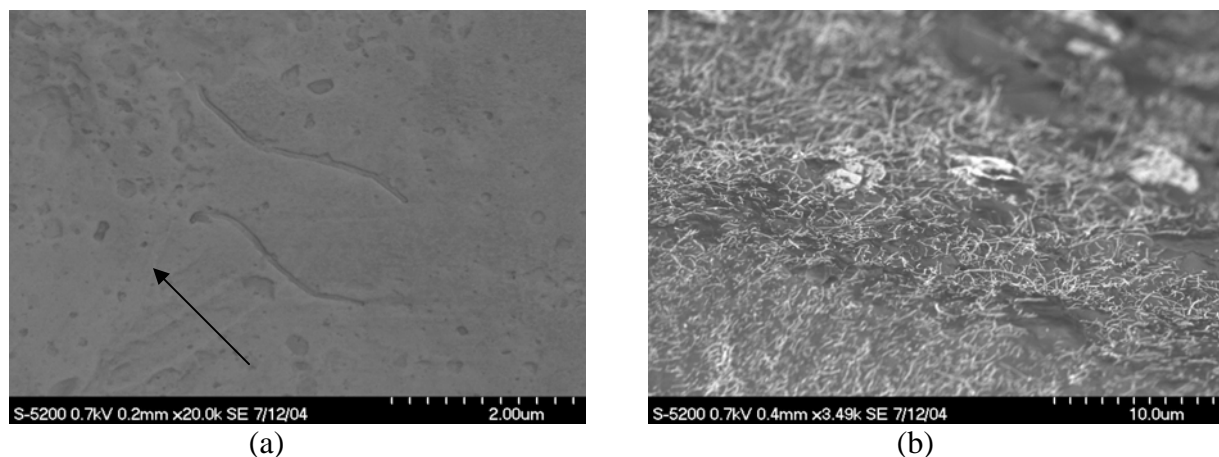


Figure 7: HRSEM of PETI-330/10 wt % MWCNT plaque (a) on the surface and (b) at the fracture (arrow indicates flow direction)



Fractured surface of PETI-330/15 wt % MWCNT



Top surface of PETI-330/10 wt % MWCNT

Fig 8: Optical microscope pictures of sample defects

Table 1: Glass transition temperatures (T_g) and temperature at 5 % weight loss:

Sample	T_g , °C	Temperature at 5 % wt loss, °C (in air)
PETI-330 (neat)	326	508
+ 3 wt % MWCNT	325	473
+ 5 wt % MWCNT	328	479
+ 7 wt % MWCNT	329	484
+ 10 wt % MWCNT	329	485
+ 12 wt % MWCNT	331	482
+ 15 wt % MWCNT	332	491
+ 20 wt % MWCNT	332	464
+ 25 wt % MWCNT	332	462

Table 2: Hardness of PETI-330/MWCNT plaques

Sample	Shore D hardness	Rockwell hardness	
		Top Surface	Bottom Surface
PETI-330 (neat)	89	84.4	84.7
+ 10 wt % MWCNT	88	79.7	79.3
+ 15 wt % MWCNT	89	78.9	79.1

Table 3: Electrical properties of PETI-330/MWCNT plaques:

Sample	Surface resistivity, Ω/cm	Surface resistivity		Volume resistivity, $\Omega\text{-cm}$
		Top Ω/sq	Bottom, Ω/sq	
PETI-330 (neat)	insulative	$> 10^{12}$	$> 10^{12}$	insulative
10 wt% MWCNT	8.86×10^3	1.8×10^4	1.9×10^4	5.5×10^4
15 wt% MWCNT	5.13×10^3	8.7×10^3	1.6×10^4	2.3×10^4

Table 4: Thermal conductivity of PETI-330/MWCNT plaques:

Sample	Thickness, mm	Specific gravity	Cp, J/gK	Diffusivity, mm^2/s	TC (W/mK)
PETI-330 (neat)	2.417	1.305	1.199	0.140	0.219
10 wt% MWCNT	2.769	1.333	1.237	0.350	0.577
15 wt% MWCNT	2.697	1.367	1.309	0.434	0.777

References:

1. D. Wilson, H.D. Stenzenberger and P.M. Hergenrother "Polyimides", Blackie and Sons Ltd., Glasgow, UK, (1990).
2. P.M. Hergenrother, High Performance Polymers, 15(1), 3 (2003).
3. J.W. Connell, J.G. Smith Jr, P.M. Hergenrother and M.L. Rommel, Intl. SAMPE Tech. Conf. Series; 30, 545 (1998).
4. J.M. Criss, J.W. Connell and J.G. Smith Jr., Intl. SAMPE Tech. Conf. Series; 30, 341 (1998).
5. J.M. Criss, C.P. Arendt, J.W. Connell, J.G. Smith Jr. and P.M. Hergenrother, SAMPE J, 36(3), 32 (2000).
6. J.G. Smith Jr, J.W. Connell, P.M. Hergenrother and J.M. Criss, Soc. Adv. Mat. Proc. Eng. Ser., 46, 510 (2001).
7. J.G. Smith Jr, J.W. Connell, P.M. Hergenrother and J.M. Criss, J. Comp. Matls; 36(19), 2255 (2002).
8. J.M. Criss, R.W. Koon, P.M. Hergenrother, J.W. Connell and J.G. Smith Jr., Intl. SAMPE Tech. Conf. Series, 33, 1009 (2001).
9. J.G. Smith Jr., J.W. Connell, P.M. Hergenrother, R. Yokota and J.M. Criss, Soc. Adv. Mat. Proc. Eng. Ser., 47, 316 (2002).
10. J.G. Smith Jr., J.W. Connell, P.M. Hergenrother, L.A. Ford and J.M. Criss, Macromol. Symp., 199, 401 (2003).
11. J.W. Connell, J.G. Smith Jr. and P.M. Hergenrother, U.S. Patent 6,359,107 B1 to NASA (2002).
12. J.M. Criss, M.A. Meador, K.C. Chuang, J.W. Connell, J.G. Smith Jr., P.M. Hergenrother and E.A. Mintz, Soc. Adv. Mat. Proc. Eng. Ser., 48, 1063 (2003).

- 13 J.W. Connell, J.G. Smith Jr., P.M. Hergenrother and J.M. Criss, High Performance Polymers, **15**, 375 (2003)
14. J.W. Connell, J.G. Smith Jr., P.M. Hergenrother and J.M. Criss, Intl. SAMPE Tech. Conf. Series, **35**, 2003.
15. J.W. Connell, J.G. Smith Jr., P.M. Hergenrother and J.M. Criss, Soc. Adv. Mat. Proc. Eng. Ser., **48**, 1076 (2003).
16. K.A. Watson, J.G. Smith Jr. and J.W. Connell, Soc. Adv. Mat. Proc. Eng. Ser., **48**: 1145 (2003).
17. C. Park, Z. Ounaies, K.A. Watson, R.E. Crooks, J.G. Smith Jr., S.E. Lowther, J.W. Connell, E.J. Siochi, J.S. Harrison and T.L. St. Clair, Chem. Phys. Lett., **364**, 303 (2002).
18. J.G. Smith Jr., J.W. Connell and P.M. Hergenrother, 46th International SAMPE Symposium and Exhibition, **46**, 510 (2001).
19. R. Haggemueller, H.H. Gommans, A.G. Rinzler, J.E. Fischer and K.I. Winey, Chem Phys Lett, **330**, 219 (2000).
20. Z. Jin, K.P. Pramoda, G. Xu and S.H. Goh, Chem Phys Lett, **337**, 43 (2001).
21. P. Potschke, T.D. Fornes and D.R. Paul, Polymer, **43**, 3247 (2002).
22. E.T. Thostenson and T. Chou, J. Phys. D: Appl. Phys., **35**, L77 (2002).
23. E.J. Siochi, D.C. Working, C. Park, P.T. Lillehei, J.H. Rouse, C.T. Topping, A.R. Bhattacharya and S. Kumar, Composites: Part B, **35**, 439 (2004).
24. Z. Konya, J. Zhu, K. Niesz, D. Mehn and I. Kiricsi, Carbon, **42**, 2001 (2004).
25. Y.A. Kim, T. Hayashi, Y. Fukai, M. Endo, T. Yanagisawa, M. Dresselhaus, Chem. Phys. Lett., **355**(3-4): 279 (2002).
26. Y.B. Li, B.Q. Wei, J. Liang, Q. Yu and D.H. Wu, Carbon, **37**, 493 (1991).
27. K. Awasthi, R. Kamalakaran, A.K. Singh and O.N. Srivastava ON. Int J Hydrogen Energy, **27**, 425 (2002).
28. J.Y. Huang, H. Yasuda and H. Mori, Chem. Phys. Lett., **303**(1-2), 130 (1999).
29. N. Pierard, A. Fonseca, Z. Konya, I. Willems, G. van Tendeloo and J.B. Nagy, Chem. Phys. Lett., **335** (1-2), 1 (2001).
30. N. Pierard, A. Fonseca, J.F. Colomer, C. Bossuot, J.M. Benoit, G. van Tendeloo and J.B. Nagy, Carbon, **42**, 1691 (2004).
31. S. Kumar, T. Uchida, T. Dang, X. Zhang and Y. Park, Soc. Adv. Mat. Proc. Eng. Ser.; **49**, (2004).
32. R. Andrews, D. Jacques, M. Minot and T. Rantell, Macromol. Mater. Eng., **287**, 395 (2002).
33. P. Potschke, A.R. Bhattacharya and A. Janke, Carbon, **42**, 965 (2004).
34. T. Ogasawara, Y. Ishida, T. Ishikawa and R. Yokota, Composites Part A, **35**, 67 (2004).
35. M. Chhowalla, K.B.K. Teo, C. Ducati, N.L. Rupesinghe, G.A.J. Amaratunga, A.C. Ferrari, D. Roy, J. Robertson and W.I. Milne, J. Appl. Phys.; **90**(10), 5308 (2001).
36. C. Stephan, T.P. Nguyen, B. Lahr, W. Blau, S. Lefrant and O. Chauvet, J. Mater. Res., **17**(2), 396 (2002).
37. J.G. Smith, Jr., K.A. Watson, J.W. Connell, D.M. Delozier, P.T. Lillehei, Y.Lin, B. Zhou, and Y.P. Sun, Polymer, **45**, 825-836 (2004).